Deformation of Sr and Rb isotopes close to the $N = Z$ line via β-decay studies using the total absorption technique

A. B. Pérez-Cerdán,[1] B. Rubio,[1,*] W. Gelletly,[2] A. Algora,[1,3] J. Agramunt,[1] E. Nácher,[1,4] J. L. Taín,[1] P. Sarriguren,[4] L. M. Fraile,[5] M. J. G. Borge,[4] L. Caballero,[1] Ph. Dessagne,[6] A. Jungclaus,[4] G. Heitz,[6] F. Marechal,[6] E. Poirier,[6] M. D. Salsac,[6] and O. Tengblad[4]

[1]*IFIC, CSIC–University of Valencia, E-46071 Valencia, Spain*
[2]*Department of Physics, University of Surrey, Guildford GU2 5XH, United Kingdom*
[3]*Institute of Nuclear Research of the Hungarian Academy of Sciences, Debrecen H-4001, Hungary*
[4]*Instituto de Estructura de la Materia, IEM-CSIC, E-28006 Madrid, Spain*
[5]*Grupo de Física Nuclear, Universidad Complutense, CEI Moncloa, E-28040 Madrid, Spain*
[6]*Institut Pluridisciplinaire Hubert Curien, IN2P3-CNRS, F-67037 Strasbourg Cedex 2, France*

(Received 20 November 2012; revised manuscript received 16 May 2013; published 26 July 2013)

A study of the Gamow-Teller strength distributions B(GT) in the beta decay of ^{78}Sr and ^{76,78}Rb has been made using a total absorption spectrometer (TAS). Following the success in deducing the sign of the deformation for ^{76}Sr, a similar approach is adopted for ^{78}Sr based on a comparison of the measured B(GT) with quasiparticle random-phase approximation calculations. This work confirms its previously expected prolate deformation in the ground state. Conclusions about the structure of the odd-odd ^{76,78}Rb isotopes have been drawn based on their measured B(GT) distributions.

DOI: 10.1103/PhysRevC.88.014324 PACS number(s): 23.40.Hc, 21.60.−n, 23.20.Lv, 27.50.+e

I. INTRODUCTION

Atomic nuclei have a wide variety of shapes in both their ground and excited states. The shapes range from spherical to superdeformed [1] and maybe even hyperdeformed spheroids [2] which are oblate or prolate. They can also have octupole deformations [3] and perhaps even more exotic shapes. In this paper we report measurements of Gamow-Teller strengths, B(GT), that are used to determine the shapes of ^{76,78}Sr and ^{76,78}Rb using the Total Absorption Spectroscopy (TAS) method [4]. The measurements are part of a programme of such studies of nuclei with masses $A = 70$–80 close to the $N = Z$ line. The reason to focus on this part of the nuclear chart is that the neutrons and protons are filling the same orbitals, and we observe rapid changes in shape with small changes in Z and N, leading to different nuclear shapes including large prolate and oblate deformations and shape coexistence involving spherical, oblate, and prolate shapes. This is consistent with the Nilsson model [5], which shows that strongly deformed oblate and prolate shapes are expected to lie lowest in energy at Z and $N = 34$, 36 (oblate) and 38 (prolate).

The primary aim of the present work was to determine and compare the shapes of the ground states of ^{76,78}Sr and ^{76,78}Rb. This was done using the TAS method [4]. The data for ^{76}Sr were analyzed previously and the results published [6]. Here we include the ^{76}Sr results for completeness. The theoretical background is based on an idea originally put forward by Hamamoto *et al*. [7], namely that the deformation of the nuclear ground state can be deduced by measuring the Gamow-Teller distribution, B(GT), in its β decay and comparing it with calculated distributions. Sarriguren *et al*. [8] then implemented the required calculations in which the B(GT) is determined for the deformations that minimize the ground state energy. It should be noted that this method works only in those cases where the predicted B(GT) distribution differs markedly for the different ground state shapes. This is the case for the light Kr and Sr nuclei.

The method demands a precise determination of the B(GT) as a function of the excitation energy in the daughter nucleus, which turns out to be a difficult task. Typically the measurements rely on studies of the beta-delayed γ rays with high purity germanium (HPGe) detectors. The beta feeding to a level in the daughter nucleus is deduced from the difference between the total intensities of the feeding and deexciting transitions. What seems a simple approach can lead to large systematic errors in complex decays since such detectors have only modest efficiency for γ rays of several MeV energy. Thus the relevant but very fragmented beta feeding to states at high excitation in the daughter nucleus often remains undetected because the resulting γ-ray decays are not seen. This is due to (a) the low photopeak efficiency for high energy γ rays, (b) the high fragmentation of the B(GT) to the states in a region of high level density, and (c) the fragmentation of the γ-ray deexcitation via many different pathways. Together these effects constitute the so-called *Pandemonium* effect [9]. As a consequence, the levels at low excitation energy are assigned an excessive beta feeding, and feeding at high excitation energy is underestimated or unobserved.

This problem can be solved using the TAS method [4] which is based on the detection of the total energy of the γ-ray cascade instead of the detection of individual γ rays. For such a purpose large inorganic scintillator crystals, such as NaI(Tl) or BaF_2, are used to create a detector with a high detection efficiency and an acceptable resolution for γ rays. Such scintillators are constructed with a geometry that covers as closely as possible a solid angle of 4π around the source

*berta.rubio@ific.uv.es

in order to provide a very high efficiency for the absorption of the complete energy in the cascades. Ideally the information on the beta feeding could be extracted directly from the measured beta-delayed γ-ray spectrum if the scintillator had a 100% full-peak efficiency for gamma detection and infinitely good γ-ray energy resolution. However the reality is far from ideal and leads to a complex problem in the analysis of the total absorption spectra. These difficulties have been assessed in [10,11], where solutions to the analysis problem are outlined.

The method has already been tested and found to work in studies of ^{76}Sr [6] and ^{74}Kr [12]. It has also been applied in reactor decay heat studies leading to the solution of a large part of the gamma discrepancy in ^{239}Pu [13] and to the input data for antineutrino spectra calculations [14]. The results reported here are for both even-even and odd-odd decays. We have the relevant theoretical calculations [15] for the even-even ^{76,78}Sr cases, and although we do not have the calculations for the daughter odd-odd cases we believe that we can also draw some conclusions about them. It is worth noting here that the odd-odd cases are cleaner from the experimental point of view, partly because the Q_{EC} values are larger than the Q_{EC} values of the even-even daughter nuclei and partly because the corresponding nuclei are either stable or very long-lived, which means that there are fewer problems due to background.

In order to analyze the data it is necessary to have some information on the discrete level structure of the nuclei concerned. Here we can rely on published information on all of the decays [16–18] except for ^{78}Sr decay, where we carried out a dedicated experiment [19] at CERN-ISOLDE to establish its decay scheme.

II. EXPERIMENTS

The beta-delayed γ rays emitted in the decay of ^{76,78}Sr and ^{76,78}Rb were measured at CERN-ISOLDE with the TAS spectrometer *Lucrecia* [4,6,12]. The measurements for mass 76 and 78 were carried out in two separate experiments which differ only slightly and are described below.

The Sr and Rb nuclei were produced in spallation reactions in Nb foil targets of thicknesses 52 g cm^{-2} (mass 76) and 37 g cm^{-2} (mass 78) under bombardment by 1.4 GeV protons delivered by the PS Booster. The PS Booster operated with a 16.8 s supercycle delivering 14 pulses of 3.2×10^{13} protons per pulse with a repetition rate of 1.2 s. The number of pulses directed on to the ISOLDE target could be varied from 2 to 9 pulses per supercycle (see Table I). After diffusion and effusion from the target the atoms were ionized in a surface ionization source.

One difficulty in the production method is the dominance of Rb ions from the surface ionization source. In order to suppress this isobaric contamination in our Sr samples, a fluorination technique was used in which Sr and F ions are combined in a molecule and then the molecule is separated from other ions in the ISOLDE mass separators (it should be noted that Rb and F ions do not combine in this way). For that purpose, CF_4 was added to the ion source carrier gas [22].

TABLE I. The half-life $T_{1/2}$ [19,20] and Q_{EC} [21] values for each isotope under study are shown. The time settings for the tape cycle—collection time T_c, delay time T_d, and mesurement time T_m—together with the typical number of proton pulses, N_p, used for the production of the different isotopes and counting rates registered in Lucrecia at the beginning of the cycle, are also specified.

Isotopes	$T_{1/2}$ (s)	Q_{EC} (keV)	T_c (s)	T_d (s)	T_m (s)	N_p	Activity (counts/s)
^{76}Sr	8.9(3)	6230(30)	15	0	15	9	4500
^{76}Rb	36.5(6)	8535(4)	15	3	12	2	4000
^{78}Sr	155(3)	3761(8)	32	0	32	2	5400
^{78}Rb	1059.6(48)	7244(3)	16.8	750	1080	5	5300

We are interested in the study of the decay of ^{78}Rb for two reasons. Firstly we are interested in the properties of this decay, and secondly we must take it into account as the daughter activity of ^{78}Sr. It turns out that ^{78}Rb has two low-lying states which beta decay, see Fig. 1, namely the 0^+ ground state and the 4^- state at 111.2 keV excitation energy. In the spallation reaction both states are populated. However ^{78}Sr produces only the 0^+ ground state (gs) as daughter activity and not the 4^- state. Therefore we have to produce the ^{78}Rb through the decay of ^{78}Sr only, i.e., using the fluorination technique. This also means that our results address the decay and hence the shape of the 0^+ ground state in ^{78}Rb. The fluorination technique was only used for the production of ^{76,78}Sr and ^{78}Rb. The fluorination technique was not used for the extraction of ^{76}Rb since, as mentioned above, it is easily ionized in the surface ionization source and no isomeric-state complication is expected. The SrF^+ and Rb^+ ions were extracted from the ion source with a 60 kV potential [23] between target and beamline (on ground potential) and analyzed by mass in the ISOLDE high resolution separator (HRS, first experiment, mass 76) and in the general purpose separator (GPS, second experiment, mass 78). The transmission from the output of the separator to the experimental setup was 78% for mass 76 and 46% for

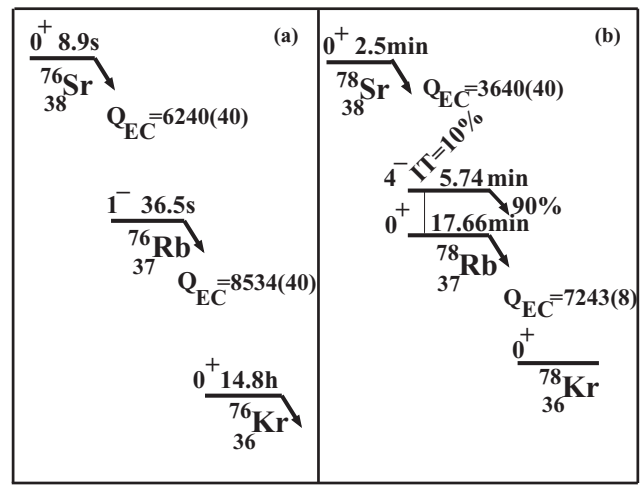

FIG. 1. Schematic picture of the β^+/EC decays of ^{76,78}Sr and ^{76,78}Rb. The Q_{EC} values and half-lives have been taken from the literature [19–21].

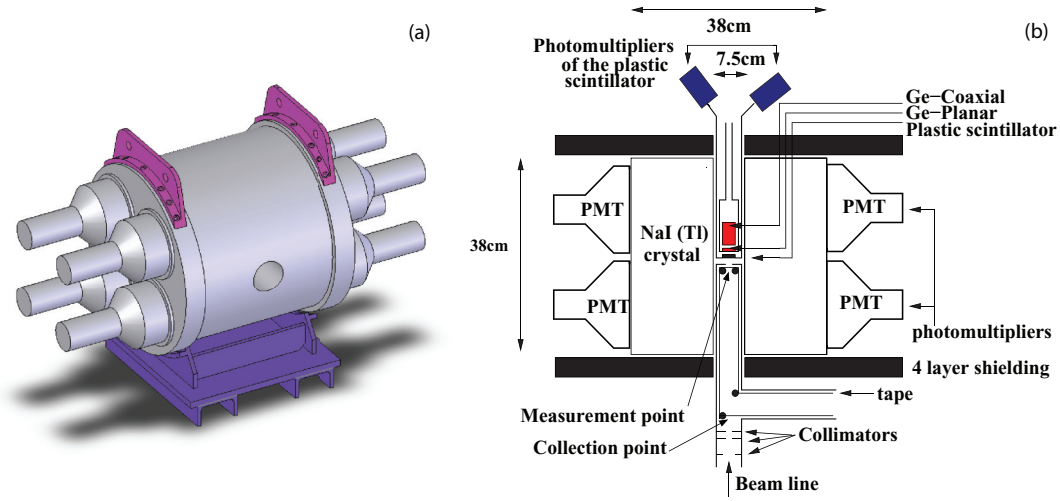

FIG. 2. (Color online) The left-hand side of the figure (a) shows a 3D picture of the TAS Lucrecia. The right-hand side (b) displays a schematic drawing of the setup showing a transverse cut through the scintillator crystal and the ancillary detectors. The setup is placed inside four layers of shielding that lowers the background caused by neutron and γ-ray activity during the bombardment of the target by the proton pulse. The beam of the separated species of interest is implanted and collected in a magnetic tape and then moved to the center of the crystal where the measurement is performed.

mass 78. The beam of radioactive ions was implanted in a 55 μm thick, aluminized mylar tape outside the experimental apparatus and transported to the measurement point, located in the middle of the spectrometer, by means of a tape transport system (Fig. 2).

In our experiments the measurements were performed with the TAS spectrometer Lucrecia. This detector was conceived and designed for the study of the β-strength function, in particular for β decays with a large Q value. It consists of a large cylindrical single crystal of NaI(Tl), 38 cm $\times$ 38 cm, covering a solid angle of $\sim 4\pi$, as shown in Fig. 2. The light coming from the scintillator material is collected by eight 5 inch coupled photomultiplier tubes (PMTs). The crystal has a transverse hole (7.5 cm in diameter) which allows the beam pipe to enter up to the center of the crystal and different ancillary detectors to be placed close to the position of the source to allow the detection of x-rays [to select the electron capture (EC) decay] and positrons/electrons (to select β decay). The crystal is encased in a 13 mm thick aluminium cylinder whose thickness gets reduced to 1.1 mm inside the radial hole in order to limit the γ-ray absorption around the source. The crystal is coated with a 2 mm thick Al_2O_3 layer to provide good light reflection. In our experiments the resolution of the NaI(Tl) crystal was 8.4% at 661.7 keV and 4.3% at 2754.0 keV. The ancillary detectors introduced into the hole were a beta counter for positrons and a germanium telescope for the detection of x rays and γ rays, as shown in Fig. 2(b). The beta counter consisted of a 2 mm thick NE102 plastic scintillator material which is placed in front of the germanium detector and close to the radioactive source. Different plastic scintillator detectors were used in the two experiments, with the solid angles covered being 14.6% and 17.3% for the experiments on the nuclei with masses 76 and 78 respectively. The main difference between them lay in the collection of the light. In the experiment on mass 76, the light collection was done via two rigid light guides, while in the second experiment these were replaced by 90 optical fibres, which made the placement of the photomultipliers easier. The germanium telescope consisted of a 1 cm thick planar Ge detector backed by a 5 cm thick coaxial Ge detector. The energy resolution for the planar detector was 0.66 keV at 59.5 keV and it covered an energy range up to 362 keV. The coaxial detector showed an energy resolution of 1.0 keV at 121.8 keV and 1.9 keV at 1112.1 keV and covered an energy range of 75–4300 keV. The end cap of the telescope cryostat was made of a thin Be window to reduce the x-ray absorption. The total solid angle covered by the telescope was approximately 17% of 4π. The whole spectrometer was isolated by a four-layer shield of boron polyethylene (10 cm), lead (5.1 cm), copper (1.5 cm), and aluminium (2 cm) which reduced the counting rate coming from the room background.

A tape transport system moved the source at a speed of 1.3 m/s from the collection point, behind the last collimator in front of Lucrecia (see Fig. 2), to the center of the crystal where the measurements were performed. Every measurement cycle was divided into three parts: the collection time (T_c), the time for the accumulation of the radioactive isotopes on the tape; the transport time that was always the same and just below 1 s, during which the source is moved to the measurement point; and the measurement time (T_m), which was decided taking into account the half-life of the nucleus to be measured and the half-life of the daughter nucleus. In the ^{76}Rb and ^{78}Rb measurements a delay time T_d was introduced before the data acquisition began. Table I shows the measurement cycles chosen for the different isotopes of interest. The data acquisition was inhibited for about 10–15 ms after the incoming proton beam to avoid the background caused by neutrons generated after the proton beam impacted on the target. A total of 780, 76, 218, and 274 min were devoted to the measurements of ^{76}Sr, ^{76}Rb, ^{78}Sr, and ^{78}Rb respectively.

Data were recorded in two different modes, directly and in listmode, using a FERA/CAMAC-VME data acquisition control system. Signals from the eight PMTs of the TAS and their sum were recorded directly together with the signals from the two PMTs of the plastic scintillator, the coaxial and the planar detectors. Coincidence timing signals from the TAS with the plastic scintillator or the planar detector and coincidences between the two PMTs of the plastic scintillator were also recorded. Background measurements were performed interspersed with the measurements on the various isotopes. Calibration measurements using standard sources, namely ^{241}Am, ^{137}Cs, and ^{60}Co, were carried out at the end of the experiment. In addition, ^{24}Na was produced at the end of both experiments and steered up to the TAS station in order to allow a check on the reproduction of the response function of Lucrecia with the Monte Carlo techniques which will be described in the following section.

III. ANALYSIS AND RESULTS

The aim of the present work is to obtain the B(GT) distribution as a function of the excitation energy in the daughter nucleus for the nuclei of interest and deduce some information on their structure. This quantity can be determined from the feeding probability I_β to a level with excitation energy E as in Eq. (1):

$$B(GT) = \frac{K \quad I_\beta(E)}{(g_A/g_V)^2 f(Q_{EC} - E) T_{1/2}} \tag{1}$$

where $K = 6143.6(17)$ [24], $g_A/g_V = -1.270(3)$ [25] is the ratio of axial-vector and vector coupling constants for the free neutron decay, $f(Q_{EC} - E)$ is the Fermi integral, and $T_{1/2}$ is the β-decay half-life in seconds. Table I summarizes the relevant measured values of $T_{1/2}$ [19,20] and Q_{EC} [21]. The term $f(Q_{EC} - E)$ can be calculated using numerical methods and can be found in tabular form [26]. Therefore, our problem lies in the determination of the feeding probability in order to extract the B(GT) distribution for the cases of interest.

In principle, there are three possible philosophies in the analysis of the TAS spectra: the spectrum can be analysed in coincidence with the x-rays (EC-component), in coincidence with the positrons (β^+-component) or one can use the singles spectrum as a whole ($\beta^+ +$ EC-component). The first and second options are cleaner since room background contamination does not need to be considered, while the third one provides higher statistics. In the particular case of coincidences with the x-rays, the isobaric contamination is eliminated. This is especially important in cases where there is strong daughter contamination. Unfortunately, in the case of ^{78}Sr, the coincidences between the x-rays and γ-rays have a large contribution from the x-rays produced following internal conversion of some highly converted, low energy transitions. The other nuclei of interest, namely ^{76}Rb and ^{78}Rb, present x-ray coincidence spectra with poor statistics due to their small EC/β^+ ratios. Consequently, these spectra were not used in the present analysis. On the other hand, the analysis of the β^+ component alone means that part of the Q-window is missing from the spectra. The last 1022 keV are of extreme importance since in the cases under study it is expected that an important part of the β-strength lies in that region. Hence, the analysis of the TAS data without any coincidences ($\beta^+ +$ EC-component) was chosen based on the arguments above.

As stated in the introduction, the most accurate way to measure the beta feeding probability I_β is often total absorption spectroscopy. Since Lucrecia has a γ-ray efficiency lower than 100% and is sensitive to β particles, its response to the β-particles and electromagnetic de-excitation cascades must be taken into account to unfold the measured data. The relation between the measured TAS spectrum **d** and the level feeding distribution **f** ($= NI_\beta$; N is the number of decays) can be represented in the following form:

$$\mathbf{d} = \mathbf{R}\mathbf{f}, \tag{2}$$

where **R** is the response function matrix of the spectrometer. Accordingly, the first step is to construct the response function of our TAS. This function includes the response of the apparatus to the different quanta emitted in the decay as well as the deexcitation branching ratios for the levels populated in the daughter nucleus [27]. The apparatus response was simulated using the Monte Carlo GEANT4 code package [28]. For such simulations an accurate description of the physical processes, the materials, and the geometry of the setup need to be considered. This involves highly detailed descriptions of the scintillator crystal including ancillary detectors, beam pipe, collimators, shielding, tape transport system, etc.

For each beta decay, the response of the detector is unique and must be constructed taking into account the level scheme of the daughter nucleus. A knowledge of the deexcitation branching ratios from the level scheme of the daughter nucleus, is thus a prerequisite in building the response matrix. For complex decay schemes with large Q values, as in the cases studied here, accurate information on low-lying excited states can only be obtained with high resolution spectroscopy. As explained before, the relevant but very fragmented strength to states at high excitation energy in the daughter nucleus often remains undetected due to the modest efficiency of Ge detectors. As a consequence, the deexcitation branching ratios are also unknown. This problem can be overcome by using the statistical model, which describes the level excitation energies, I^π values, and the electromagnetic deexcitation for the corresponding part of the level scheme where no experimental data are available. This statistical model uses average quantities such as level densities and strength functions [29]. On the one hand, the level excitation energies, parities, and spins are derived within the statistical model using a parametrization of the back-shifted Fermi-gas (BSFG) formula [30], which depends on a (MeV^{-1}), the level density parameter, and Δ (MeV), a fictive ground-state. The parameters a and Δ are nucleus dependent and are usually adjusted in order to reproduce experimental level densities. Since they were not available experimentally for the nuclei of interest, they were obtained using the total nuclear level density derived from realistic microscopic single-particle level schemes determined within HF-BCS calculations [29]. Different quadrupole deformations for the ground state were considered in these calculations, in particular those deformations that are predicted by the theory. On the other hand, the deexcitation branching ratios

are obtained from gamma-strength functions related to the nuclear giant resonance excitation modes by the Axel-Brink hypothesis [31]. These strength functions depend on E_0 (MeV), Γ_0, and σ_0, the giant resonance parameters. These three parameters can be extracted from the systematics [32–34]. Only transitions of $E1$, $M1$, or $E2$ type were considered in our work. In the case of $E1$ transitions, two possible parametrizations are available for deformed nuclei with $A > 50$, and both of them were considered. In addition, since they depend on the deformation, different assumptions for the deformation were made according to the values predicted by the theory for the nuclei of interest.

In this work, the branching ratios can be obtained empirically up to a certain level in the known part of the level scheme. Hence, the levels and γ-ray transitions have a well defined value. For the unknown part, where the branching ratios were derived from the statistical model we grouped the levels into bins of 40 keV up to the Q_{EC} value. This made it possible to overcome the intractable problem of the convolution of the different quanta in the region of high level density. However, this approximation introduces systematic errors in the determination of the beta strength. These effects have been extensively investigated in [10].

The β^+ particles were simulated with the corresponding endpoints for each nucleus. We also simulated the exact energies of the gamma-ray transitions for the known part of the level scheme. Average energies (multiples of the energy bin width of 40 keV) were used in the Monte Carlo simulations of the γ-ray response functions for the unknown part. The nonproportional light yield for gamma rays observed in a TAS [35] was also taken into account in the simulations.

As mentioned before, ^{24}Na was produced *in situ* at ISOLDE after the Sr and Rb isotope production runs were completed in order to validate our Monte Carlo simulations. The fact that this source was produced under exactly the same conditions as the nuclei of interest in this work ensures the reproduction of the source position and size. The beta decay of ^{24}Na is rather simple and well known with a large Q_β window, consisting mainly of one cascade with two γ rays as shown schematically in Fig. 3. In this work, its decay was simulated and compared to the experimental spectrum. Figure 3 shows how well the measured ^{24}Na spectrum is reproduced using the GEANT4 code.

The construction of the response function of the detector for the decay of ^{78}Sr needed further consideration. The occurrence of the 46.9 keV isomer in the de-excitation level scheme of ^{78}Rb [19] with 610(100) ns [36] introduces a temporary break in the development of the γ-ray cascade which alters the measured spectrum. For a very long-lived isomer it is equivalent to the termination of the cascade and can be easily taken into account by setting the branching ratio from that level to zero. However, for this particular case the half-life is comparable with electronic processing times and some care must be taken. Part of the cascade below the isomer will be added to the rest depending on the time delay and the pulse processing. The basic mechanism is conceptually the same as for the electronic pulse pileup distortion since the time distribution is governed by the same law, the Poisson time distribution, because the difference in the heights of the two signals is

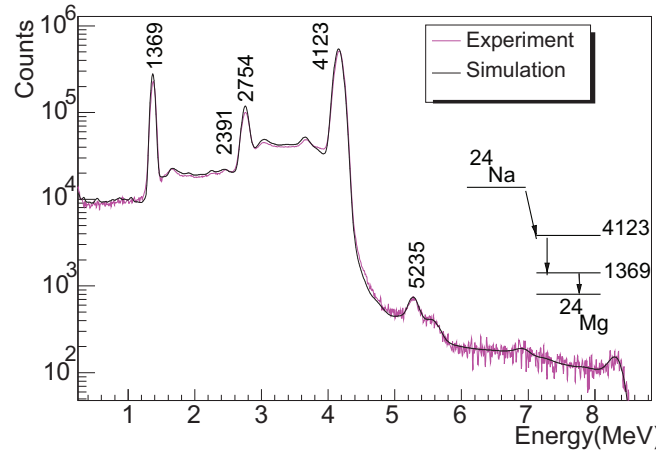

FIG. 3. (Color online) Simulation of the ^{24}Na source spectrum (black line) obtained with the GEATN4 code, overlaid with the experimental spectrum (pink line).

not randomly selected but has specific values. The probability of the summing of the post-isomeric transition with the rest of the cascade has been studied and its γ-ray response function altered accordingly. This γ-ray response has then been convoluted with the responses of the remaining quanta for the construction of the total response of the detector for this particular decay.

The raw experimental spectra suffered from various distortions, namely room background, the electronic pile-up and the contamination produced by the subsequent daughter activity, which introduced undesired counts in the spectra. In order to analyze the TAS data, the contributions of these unwanted components must be known *a priori*. The measurement of ^{78}Sr [$T_{1/2} = 155(3)$ s] [19] is clearly affected by the presence of the ^{78}Rb [$T_{1/2} = 1059.6(48)$ s] daughter activity. In order to subtract this contribution one needs to obtain a "clean" ^{78}Rb TAS spectrum. This was done using the same production procedure as for ^{78}Sr but adjusting the cycle to the ^{78}Rb half-life. The acquisition of the data started 750 s, the so-called delay time, after the source was positioned at the measurement point. This delay time was equivalent to approximately five times the ^{78}Sr half-life. The corresponding spectrum is shown in the upper panel of Fig. 4 together with the background contribution and the electronic pileup. The latter contribution was calculated by numerical methods [35]. The lower part of Fig. 4 shows the ^{78}Rb spectrum free of contaminants once they have been subtracted. Since the daughter nucleus in the ^{78}Rb decay is stable, it does not need to be taken into account as a contaminant. Turning to the ^{78}Sr case, first background and pileup were removed. The daughter activity produced following ^{78}Rb decay was then subtracted by fitting the ^{78}Rb spectrum free of contaminants (see lower part of Fig. 4) to the upper part of the ^{78}Sr spectrum in Fig. 5. The same procedure for contaminant subtraction was used in the case of ^{76}Rb.

The solution of Eq. (2) is not trivial since this is a typical "ill posed" problem. Tain and Cano-Ott [11] explored three different algorithms in order to find the solution for Eq. (2) relevant to TAS measurements. In this work we have chosen the iterative expectation-maximization (EM) method [11] to

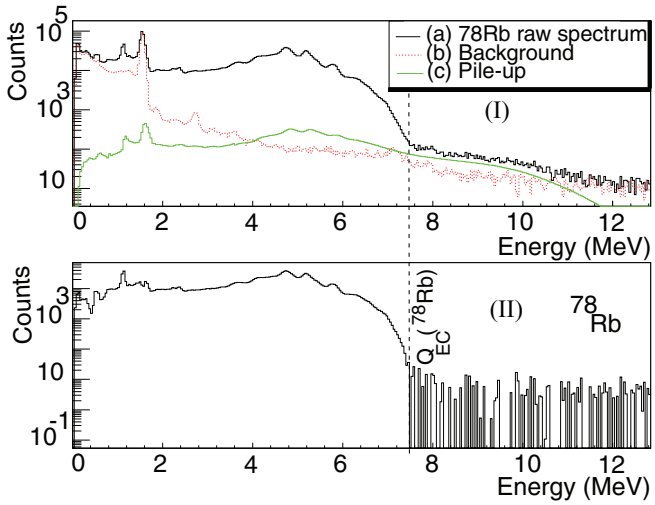

FIG. 4. (Color online) The upper part (I) of the figure shows (a) the total recorded spectrum in the TAS for the ^{78}Rb β-decay. (b) indicates the background recorded activity with no source inside Lucrecia but otherwise recorded in identical conditions. The background measurement was interspersed with the real measurement. (c) calculated pile-up (see text). The lower part (II) of the figure shows the result of (a) minus (b) and (c).

unfold the data. As can be seen in Fig. 5, after the subtraction of the undesired components the TAS spectrum shows a region, close to the Q_{EC} value, with poor statistics and channels with zero (and even negative counts). This region is quite critical to the determination of the strength since here the Fermi integral takes values close to zero due to its strong dependence on the transition energy E. Therefore, small fluctuations in the data can lead to large errors in the beta strength calculation. On the other hand, the EM method can only deal with positive counts in the spectrum. As a consequence the raw spectra were used in the analysis, which included the different contaminant

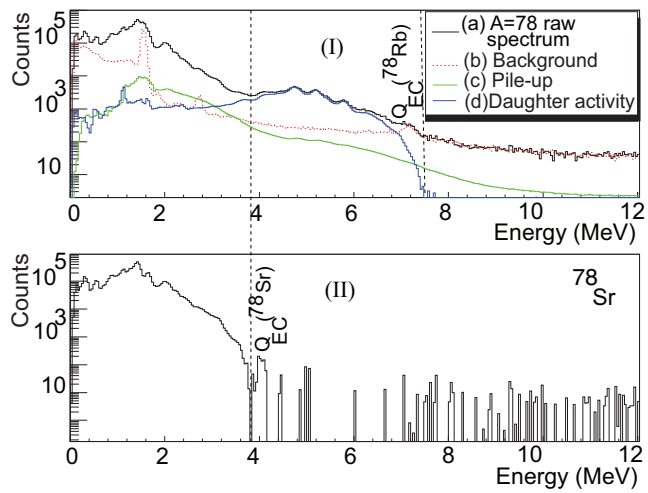

FIG. 5. (Color online) (I) Same as in Fig. 4 but for the case of ^{78}Sr β decay. Plot (d) corresponds to the daughter activity obtained in Fig. 4. The lower part (II) of the figure shows the result of (a) minus (b), (c), and (d).

components and their contributions, as well as the pileup contribution [37].

Figure 6 shows the comparison of the reconstructed spectra, using the resulting I_β obtained from the last iteration when applying the EM algorithm (grey), with the measured spectra (black) for the three cases of interest and including ^{76}Sr. As mentioned in the introduction, the ^{76}Sr results were presented in an earlier publication [6] and are shown here for completeness. As an aid to seeing the differences more clearly, the deviation between the reconstructed spectrum and the experimental one relative to the latter has also been plotted in each case. The observed larger differences in the lower energy part of the spectrum are caused by a possible mismatch between the energy calibrations of the two spectra. In addition, the limited energy resolution of the TAS makes it difficult to follow the variation of the feeding for such low energies where the density of levels is low. However, an excellent agreement can be observed in the rest of the spectra which implies that our method is reliable.

As explained above, the experimental I_β is one of the main factors contributing to the B(GT) and the main output of the present paper. Given its importance and the fact that the other two ingredients, namely the $T_{1/2}$ and the Q_β, can be remeasured in the future we present the values of the I_β for the three cases determined in this work in a tabular form. They are presented in Tables II–IV and correspond to the last iteration after applying the EM algorithm. In determining the error in I_β we have considered several factors, namely (a) the various deformations assumed for the unknown part of the level scheme where the BSFG formula is used; (b) the two possible parametrizations of the strength function of $E1$ gamma radiation which are used within the statistical model and also depend on the various deformations assumed; (c) the different assumptions made about the position of the last level (the cutoff) defining the complete knowledge of the decay scheme from the high resolution experiments; (d) the uncertainties in the normalization factor used to subtract the contaminants; and (e) the statistical error in the feeding distribution.

Before we proceed to the discussion of the B(GT) we will briefly discuss the I_β for the ground state (gs) to ground state transition which is not a trivial quantity to measure in beta decay. This is because, in contrast to the feeding to any other level, there is no characteristic gamma radiation associated with it. In our experiments however, the annihilation of positrons produces two gamma quanta with 511 keV energy which have a high probability of being absorbed in the TAS. In other words, our setup is sensitive to all beta plus decays including the gs-to-gs transition. In our study we have not included this possibility in the decay of either ^{76}Sr or ^{76}Rb since the transitions involved are first forbidden. This is not the case in the decay of the ^{78}Sr gs to the ^{78}Rb gs (0^+ to 0^+) or in the decay of the ^{78}Rb gs to the ^{78}Kr gs (0^+ to 0^+). In consequence we have included this possibility in our analysis. In both cases the best chi-square value was obtained for feeding close to zero (see Tables II and III). This is not surprising since they are both isospin-forbidden transitions. We note that our result is in contradiction with the 8% value reported by Bavaria *et al.* [18] for the case of the ^{78}Rb decay, where this result is

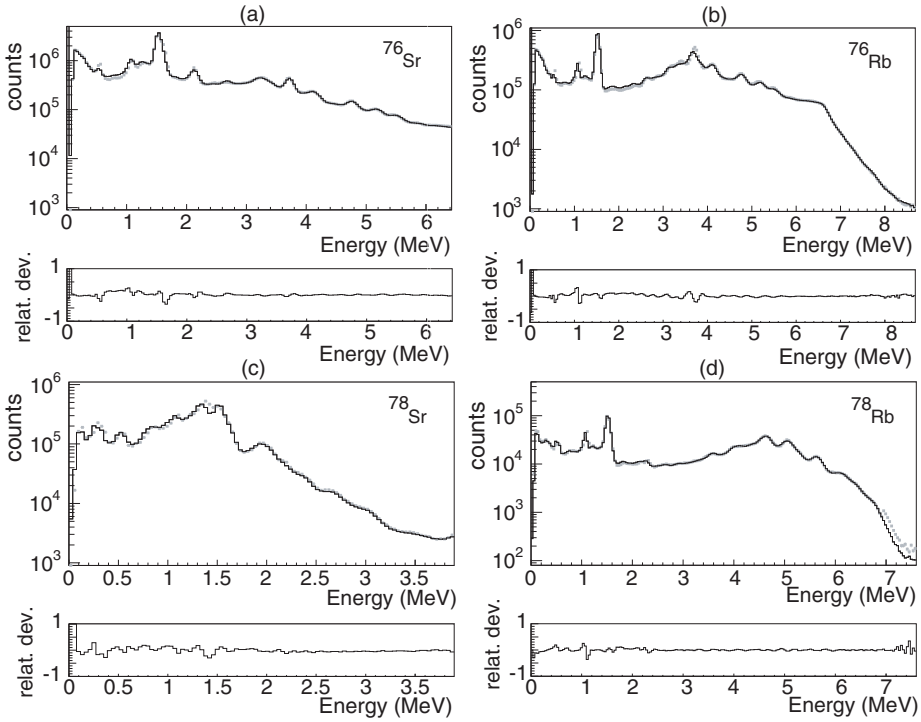

FIG. 6. Upper panels: The experimental TAS spectra for the ^{76,78}Sr and ^{76,78}Rb isotopes (black continuous line) are presented in (a), (c), (b), and (d) respectively. The reconstructed spectra obtained from our analysis appear overlaid (grey dashed lines). The associated lower panels: difference between the reconstructed spectra and the experimental spectra relative to the latter for the four cases.

discussed in terms of possible isospin mixing. We believe that this is an apparent feeding due to the Pandemonium effect as often happens when Ge detectors are used to deduce the beta feeding in complex decays.

The B(GT) distributions derived from our analyses using Eq. (1) are shown in Fig. 7 and compared with those obtained from high resolution spectroscopy. The Pandemonium effect can be clearly observed in the figure, since it results in a shift in the β strength to lower energies in the high resolution measurements. The experimental error in B(GT) arises because of uncertainties in the determination of I_β, $T_{1/2}$, and Q_{EC}. The resulting error in the B(GT) for each energy was calculated by propagating quadratically these three errors. The results are shown as shaded grey areas in the four panels of Fig. 7.

As an example of how sensitive the determination of the B(GT) is to the level scheme assumptions, we show the case of ^{78}Sr in Fig. 8. The accumulated B(GT) strength is shown in order to illustrate the problem clearly. Firstly the reader should note that there is a gap in the decay scheme of ^{78}Sr into ^{78}Rb with no levels known to be populated between 1283 and 1738 keV excitation energy [19]. Secondly the last level known in this decay scheme lies at 1951 keV. This does not mean, of course, that our knowledge of the level scheme is complete up to this level. Based on these premises we have analyzed the data assuming the cutoff of the known level scheme occurs at (a) 1283 keV, (b) 1738 keV, and (c) 1951 keV. In case (a) this means that we allow the statistical model to "fill" the gap with possible levels receiving feeding in this energy interval. In cases (b) and (c) we assume that our knowledge of the level scheme is complete up to 1738 and 1951 keV respectively. Of these three assumptions we know that the first one is wrong, option (b) is probably close to reality, and (c) is probably wrong to some extent. In consequence, we have used option (b) for our analysis.

Looking now at Fig. 8 we see that option (a) produces unphysical feeding in the energy gap. Moreover, the accumulated B(GT) is very different from the B(GT) corresponding to the other two assumptions, especially in the energy interval between 1.3 and 2.5 MeV. Options (b) and (c) do not differ much, although some difference can be seen at high excitation energy. As mentioned above, we have chosen option (b) for our analysis, however, option (c) is included in the calculation of the error in the B(GT) strength shown in Figs. 7 and 10.

It should be noted that the total accumulated B(GT) is very similar in all three cases. This is a consequence of the high efficiency of the Lucrecia spectrometer for gamma-ray cascades. But, of course, if we want to have a precise value of the B(GT) in different regions of excitation energy, then the better our knowledge of the decay scheme, the better the determination of the strength we obtain [10].

IV. DISCUSSION

The nuclei with N $\sim$ Z and mass around 80 have drawn the interest of both theoreticians and experimentalists in recent decades due to their remarkable features. The low single-particle density at the Fermi level, the presence of energy-gaps co-existing at the same excitation energy for different quadrupole deformations and the fact that the protons and neutrons are filling the same shells result in rapid changes in shape with the addition or subtraction of a single nucleon. Hence, large deformations and even shape co-existence are predicted leading to efforts to map out the deformation in the region.

TABLE II. The table shows the feeding obtained in the decay of ^{78}Sr after applying the EM algorithm for each energy level up to 1738.9 keV and for every 40 keV interval above this energy. The upper and lower errors are shown in columns 3 and 4 and are explained in the text. Feeding values below 10^{-4}% are set to 0.

Energy (keV)	Feeding (%)	Error (+)	Error (−)
0	0		
46.9	0		
103.3	0		
134.0	0		
160.8	0		
193.0	0		
255.3	4.95×10^{-3}	8×10^{-5}	1.5×10^{-4}
290.2	0.65	0.02	0.04
315.2	50.4	0.6	0.4
504.7	21.2	0.8	0.2
561.3	4.3	0.3	0.2
801.6	0.32	0.028	0.016
826.3	1.5	0.2	0.7
830.1	3.8	0.20	0.80
895.7	4.90	0.20	1.90
933.7	0.60	0.20	0.80
1038.5	3.92	0.27	0.10
1194.1	0.30	0.02	0.08
1283.4	2.40	0.02	0.50
1738.9	0.099	0.188	0.012
1780	0.0015	2×10^{-4}	2×10^{-4}
1820	0.0005	2×10^{-4}	3×10^{-4}
1860	0.00089	3×10^{-5}	2×10^{-5}
1900	0.0048	2×10^{-4}	2×10^{-4}
1940	0.041	3×10^{-3}	2×10^{-3}
1980	0.18765	1.2×10^{-4}	0.15810
2020	0.23729	1.6×10^{-4}	0.17056
2060	0.11845	2×10^{-4}	0.0426
2100	0.0802	0.0519	6×10^{-4}
2140	0.15343	0.09423	1.3×10^{-4}
2180	0.5158	0.0934	9×10^{-4}
2220	0.7211	7×10^{-4}	0.0381
2260	0.3226	0.0350	3×10^{-4}
2300	0.07509	0.03531	8×10^{-5}
2340	0.03439	0.02710	4×10^{-5}
2380	0.0381	0.0287	1.1×10^{-3}
2420	0.084	0.029	0.011
2460	0.1751	2×10^{-4}	0.0329
2500	0.2021	3×10^{-4}	0.0391
2540	0.1793	2×10^{-4}	0.0269
2580	0.1761	3×10^{-4}	0.0163
2620	0.2033	3×10^{-4}	0.0142
2660	0.2363	4×10^{-4}	0.0265
2700	0.2341	4×10^{-4}	0.0467
2740	0.1987	3×10^{-4}	0.0541
2780	0.1463	2×10^{-4}	0.0432
2820	0.1147	2×10^{-4}	0.0308
2860	0.09862	1.8×10^{-4}	0.02574
2900	0.0998	2×10^{-4}	0.0346
2940	0.1077	2×10^{-4}	0.0549
2980	0.1210	2×10^{-4}	0.0828
3020	0.1253	3×10^{-4}	0.0828
3060	0.1010	2×10^{-4}	0.0585
3100	6.854×10^{-2}	1.5×10^{-4}	2.447×10^{-2}
3140	4.354×10^{-2}	1.0×10^{-4}	1.75×10^{-3}
3180	3.135×10^{-2}	6.01×10^{-3}	8×10^{-5}
3220	2.439×10^{-2}	4.79×10^{-3}	6×10^{-5}
3260	2.205×10^{-2}	1.72×10^{-3}	6×10^{-5}
3300	2.037×10^{-2}	5×10^{-5}	1.49×10^{-3}
3340	2.156×10^{-2}	6×10^{-5}	2.06×10^{-3}
3380	2.256×10^{-2}	6×10^{-5}	1.73×10^{-3}
3420	1.992×10^{-2}	6×10^{-5}	1.10×10^{-3}
3460	1.257×10^{-2}	3×10^{-5}	7.8×10^{-4}
3500	5.952×10^{-3}	1.7×10^{-5}	5.69×10^{-4}
3540	2.357×10^{-3}	7×10^{-6}	3.35×10^{-4}
3580	9.66×10^{-4}	3×10^{-6}	1.82×10^{-4}
3620	4.65×10^{-4}	2×10^{-6}	1.10×10^{-4}
3660	2.965×10^{-4}	9×10^{-7}	8.42×10^{-5}
3700	2.580×10^{-4}	8×10^{-7}	8.83×10^{-5}
3740	3.15×10^{-4}	9×10^{-7}	1.27×10^{-4}
3780	4.70×10^{-4}	1.2×10^{-6}	2.17×10^{-4}

A. ^{78}Sr

One of the key aims of these experiments was to determine the shape of the ^{78}Sr ground state. Since the spin of the ground state is $I = 0$, no experimental quadrupole moment can be observed. Previous studies based on the measured $B(E2; 2^+ \rightarrow 0^+)$ for the ground-state band in ^{78}Sr [38] and isotope shift measurements [39] support a large deformation for the ground state of ^{78}Sr. They are in agreement with theoretical calculations which predict a large prolate deformation reported by Möller and Nix [40]. However, the experimental studies cannot give conclusive evidence on the sign of the deformation. Challenged by the success in deducing the deformation of the even-even ^{74}Kr [12] and ^{76}Sr [6] nuclei using the TAS method, we use a similar approach for ^{78}Sr, comparing our data with the existing theoretical calculations. These calculations use a self-consistent formalism based on a deformed Hartree-Fock (HF) mean field obtained with a Skyrme interaction including pairing correlations in the BCS approximation. The minimization of the HF energy can lead to different local minima corresponding to different values of the deformation for the ground state. In the case of ^{78}Sr two minima are obtained [15], one spherical and the other prolate with $\beta \sim 0.4$. Three different Skyrme forces, namely SG2, Sk3, and SLy4, have been used. They predict similar minima in the plot of the total HF energy versus deformation. A separable spin-isospin residual interaction is then added to the mean field and treated in the quasiparticle random phase approximation (QRPA) formalism to obtain the B(GT) distribution which is compared with our data. The parent ground state and the states populated in the decay are assumed to have the same deformation in the calculations.

For the comparison between the experiment and the theory we show the B(GT) as a function of the excitation energy in the daughter nucleus in Fig. 9 (left) for the SG2 force. The choice of this particular force was taken in order to be consistent with our previous study on the structure of the low-lying levels in

TABLE III. The table shows the feeding obtained in the decay of ^{78}Rb after applying the EM algorithm for each energy level up to 3662.1 keV and for every 40 keV interval above this energy. The upper and lower errors are shown in columns 3 and 4 and are explained in the text. Feeding values below 10^{-4} % are set to 0.

Energy (keV)	Feeding (%)	Error (+)	Error (−)
0	0.005	0.002	0.007
455.0	0.08	0.18	0.08
1017.2	0		
1119.5	0.000375	0.000003	0.0004
1147.9	0.00206	0.00002	0.002
1564.6	0.0679	0.0006	0.068
1755.8	0.1254	0.0013	0.12
1772.9	0.1560	0.0016	0.14
2007.3	0.1759	0.0018	0.15
2234.1	0.3140	0.003	0.19
2240.6	0.511	0.005	0.2
2399.0	0.4	0.004	0.2
2443.3	0.5880	0.006	0.3
2508.0	0.7	0.10	0.14
2573.3	0.430	0.004	0.06
2656.1	0.63	0.10	0.19
2882.5	1.94	0.02	1.0
2992.5	1.389	0.017	0.8
3230.3	2.36	0.03	1.0
3437.3	7.87	1.3	0.19
3539.0	6.7	0.9	0.5
3575.1	7.45	2.0	0.10
3662.2	1.92	0.14	0.4
3700	1.27	0.02	0.02
3740	0.762	0.007	0.012
3780	0.704	0.004	0.010
3820	1.093	0.005	0.02
3860	2.30	0.005	0.04
3900	4.33	0.011	0.07
3940	5.27	0.008	0.08
3980	3.99	0.008	0.06
4020	2.44	0.006	0.04
4060	1.71	0.004	0.03
4100	1.62	0.003	0.03
4140	1.80	0.003	0.03
4180	1.80	0.003	0.03
4220	1.36	0.002	0.02
4260	0.858	0.013	0.013
4300	0.568	0.009	0.009
4340	0.490	0.008	0.008
4380	0.596	0.010	0.010
4420	0.964	1.0	0.017
4460	1.68	0.03	0.03
4500	2.43	0.05	0.05
4540	2.50	0.05	0.05
4580	1.85	0.03	0.03
4620	1.16	0.46	0.02
4660	0.746	0.014	0.062
4700	0.516	0.010	0.07
4740	0.369	0.04	0.007
4780	0.263	0.14	0.005
4820	0.204	0.17	0.004
4860	0.206	0.16	0.004
4900	0.308	0.12	0.006
4940	0.631	0.04	0.012
4980	1.25	1.5	0.14
5020	1.70	0.03	0.12
5060	1.46	0.6	0.03
5100	0.969	0.15	0.018
5140	0.702	0.12	0.013
5180	0.637	0.16	0.012
5220	0.644	0.12	0.012
5260	0.557	0.08	0.011
5300	0.364	0.11	0.007
5340	0.202	0.13	0.004
5380	0.125	0.12	0.002
5420	0.112	0.05	0.002
5460	0.160	0.04	0.002
5500	0.299	0.8	0.005
5540	0.602	1.9	0.009
5580	0.896	1.46	0.014
5620	0.775	1.1	0.012
5660	0.432	0.7	0.007
5700	0.21	0.4	0.08
5740	0.12	0.19	0.09
5780	0.11	0.13	0.09
5820	0.16	0.12	0.13
5860	0.25	0.12	0.19
5900	0.36	0.12	0.2
5940	0.39	0.11	0.18
5980	0.35	0.10	0.15
6020	0.29	0.09	0.15
6060	0.25	0.07	0.16
6100	0.23	0.05	0.17
6140	0.229	0.011	0.18
6180	0.236	0.004	0.20
6220	0.257	0.004	0.2
6260	0.296	0.006	0.2
6300	0.349	0.004	0.3
6340	0.383	0.007	0.3
6380	0.365	0.007	0.2
6420	0.301	0.008	0.19
6460	0.233	0.004	0.14
6500	0.194	0.005	0.11
6540	0.184	0.004	0.10
6580	0.202	0.006	0.09
6620	0.241	0.007	0.12
6660	0.274	0.005	0.13
6700	0.262	0.005	0.10
6740	0.197	0.012	0.04
6780	0.126	0.005	0.007
6820	0.081	0.003	0.009
6860	0.061	0.002	0.011
6900	0.057	0.003	0.015
6940	0.057	0.003	0.016
6980	0.047	0.003	0.011
7020	0.027	0.003	0.004
7060	0.0114	0.0014	0.0013
7100	0.0045	0.0006	0.0012
7140	0.0025	0.0005	0.0014
7180	0.0024	0.0007	0.002
7220	0.004	0.006	0.009
7260	0.00998	0.00005	0.008

TABLE IV. The table shows the feeding obtained in the decay of ^{76}Rb after applying the EM algorithm for each energy level up to 3672.1 keV and for every 40 keV interval above this energy. The upper and lower errors are shown in columns 3 and 4 and are explained in the text. Feeding values below 10^{-4}% are set to 0.

Energy (keV)	Feeding (%)	Error (+)	Error (−)
424.0	0		
769.9	0		
1034.5	0		
1221.7	0		
1598.0	0		
1687.3	0		
1733.3	0		
2091.1	7.43×10^{-4}	1.5×10^{-5}	1.2×10^{-5}
2104.3	9.8×10^{-3}	2×10^{-4}	4×10^{-4}
2140.5	6.72×10^{-4}	3×10^{-5}	1.1×10^{-5}
2192.4	0.116	0.401	0.012
2227.2	0.013	0.002	0.002
2257.4	0.015	0.002	0.003
2332.6	0.34	0.03	0.02
2571.0	15.5	0.5	0.3
2581.0	6.02	0.10	1.71
2700.4	5.5	0.3	0.8
2742.3	2.09	0.04	0.91
2774.9	0.26	0.06	0.02
2816.7	0.788	0.022	0.013
2926.5	4.0	0.7	0.2
2970.0	3.94	0.41	0.07
3024.2	11.74	0.19	0.42
3242.2	1.29	0.22	0.02
3275.9	0.46	0.21	0.05
3421.5	0.17	0.11	0.03
3455.9	1.20	0.15	0.06
3602.6	2.24	0.71	0.04
3672.1	9.7	1.6	0.6
3700	0.61	0.02	0.02
3740	0.25	0.03	0.02
3780	0.13	0.02	0.02
3820	0.12	0.02	0.03
3860	0.17	0.02	0.02
3900	0.293	0.011	0.009
3940	0.49	0.15	0.02
3980	0.71	0.11	0.17
4020	0.85	0.3	0.02
4060	0.83	0.09	0.02
4100	0.74	0.02	0.02
4140	0.61	0.03	0.02
4180	0.54	0.02	0.02
4220	0.53	0.030	0.02
4260	0.61	0.2	0.02
4300	0.782	0.014	0.014
4340	1.0	0.7	0.3
4380	1.064	0.018	0.512
4420	0.909	0.016	0.411
4460	0.665	0.012	0.321
4500	0.468	0.008	0.212
4540	0.373	0.006	0.140
4580	0.355	0.006	0.101
4620	0.384	0.007	0.111
4660	0.447	0.008	0.142
4700	0.477	0.008	0.161
4740	0.462	0.008	0.142
4780	0.412	0.007	0.103
4820	0.348	0.011	0.041
4860	0.305	0.009	0.006
4900	0.291	0.021	0.017
4940	0.30	0.02	0.04
4980	0.323	0.006	0.071
5020	0.364	0.007	0.102
5060	0.412	0.007	0.121
5100	0.446	0.008	0.111
5140	0.471	0.008	0.072
5180	0.491	0.04	0.009
5220	0.520	0.081	0.009
5260	0.562	0.122	0.010
5300	0.635	0.101	0.011
5340	0.759	0.015	0.052
5380	0.945	0.017	0.171
5420	1.13	0.02	0.32
5460	1.21	0.02	0.42
5500	1.09	0.02	0.31
5540	0.84	0.05	0.15
5580	0.60	0.06	0.07
5620	0.43	0.05	0.05
5660	0.33	0.04	0.04
5700	0.28	0.02	0.041
5740	0.260	0.007	0.040
5780	0.247	0.005	0.043
5820	0.228	0.004	0.040
5860	0.201	0.004	0.041
5900	0.164	0.005	0.032
5940	0.136	0.010	0.033
5980	0.115	0.012	0.019
6020	0.105	0.012	0.012
6060	0.102	0.012	0.007
6100	0.104	0.011	0.004
6140	0.107	0.007	0.007
6180	0.110	0.002	0.010
6220	0.110	0.002	0.015
6260	0.106	0.002	0.016
7340	7.32×10^{-3}	6.01×10^{-3}	1.3×10^{-4}
7380	3.38×10^{-3}	3.22×10^{-3}	6×10^{-5}
7420	1.53×10^{-3}	1.22×10^{-3}	3×10^{-5}
7460	7.3×10^{-4}	1.3×10^{-4}	5×10^{-5}
7500	3.73×10^{-4}	7×10^{-6}	1.22×10^{-4}
7540	2.12×10^{-4}	4×10^{-6}	1.33×10^{-4}
7580	1.35×10^{-4}	2×10^{-6}	1.02×10^{-4}
7620	1.01×10^{-4}	2×10^{-6}	9.1×10^{-5}
7660	9.26×10^{-5}	1.8×10^{-6}	8.23×10^{-5}
7700	1.08×10^{-4}	2×10^{-6}	9.1×10^{-5}
7740	1.62×10^{-4}	3×10^{-6}	1.32×10^{-4}
7780	3.09×10^{-4}	7×10^{-6}	2.11×10^{-4}
7820	7.01×10^{-4}	1.3×10^{-5}	4.31×10^{-4}
7860	1.68×10^{-3}	4×10^{-5}	6.1×10^{-4}
7900	3.75×10^{-3}	8×10^{-5}	7.3×10^{-4}
7940	6.7×10^{-3}	9×10^{-4}	6×10^{-4}
7980	9.0×10^{-3}	1.4×10^{-3}	4×10^{-4}
8020	9.2×10^{-3}	5×10^{-4}	2×10^{-4}

TABLE IV. *(Continued.)*

Energy (keV)	Feeding (%)	Error (+)	Error (−)
8060	7.7×10^{-3}	2×10^{-4}	6×10^{-4}
8100	5.69×10^{-3}	1.5×10^{-4}	2.1×10^{-4}
8140	3.82×10^{-3}	1.0×10^{-3}	2×10^{-4}
8180	2.34×10^{-3}	1.40×10^{-3}	1.2×10^{-4}
8220	1.31×10^{-3}	1.01×10^{-3}	8×10^{-5}
8260	6.98×10^{-4}	3.2×10^{-4}	5×10^{-5}
8300	3.95×10^{-4}	1.6×10^{-5}	7.1×10^{-5}
8340	2.73×10^{-4}	1.3×10^{-5}	1.72×10^{-4}
8380	2.62×10^{-4}	1.5×10^{-5}	2.23×10^{-4}
8420	3.5×10^{-4}	3×10^{-5}	3.1×10^{-4}
8460	6.2×10^{-4}	9×10^{-5}	6.2×10^{-4}
8500	1.2×10^{-3}	4×10^{-4}	1.4×10^{-3}
8540	2.1×10^{-3}	1.0×10^{-2}	1.2×10^{-2}

the daughter nucleus ^{76}Rb [19]. A standard quenching factor of 0.6 has been included in the calculations. We see that the calculated strength distribution is concentrated in only a few peaks in comparison with the measured one which is much more fragmented. This could be an indication of the missing correlations not taken into account in the present model which is a well known feature of QRPA calculations. The theoretical distributions folded with 0.5 MeV width Gaussians shown at the right of Fig. 9 effectively simulate this fragmentation. One observes two regions below 3 MeV with concentrations of strength that correspond to the measured distribution, although the exact position of the levels with strong feeding is not well reproduced.

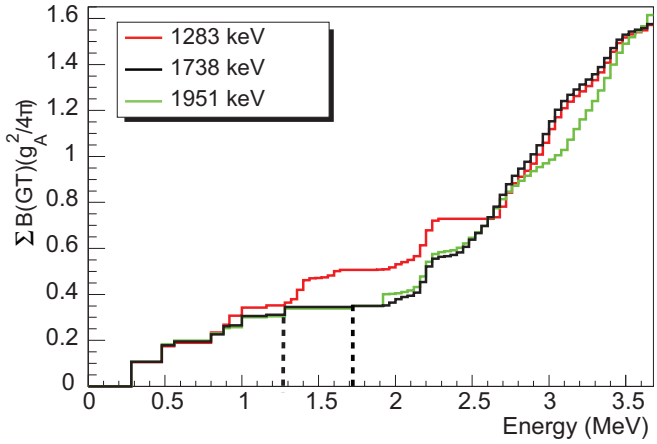

FIG. 8. (Color online) Accumulated B(GT) for the decay of ^{78}Sr obtained from different assumptions on the position of the last level supposed to be known in its decay scheme [19]. The vertical dashed lines indicate the gap in the decay scheme of ^{78}Sr into ^{78}Rb with no levels populated [19].

The main difference in the two calculations is that the prolate case predicts larger strength in the upper region. In order to see how the two calculations compare with experiment it is better to plot the accumulated B(GT) as a function of energy as shown in Fig. 10, where we have now included the results for other Skyrme forces, namely SK3 and SLy4. Although the calculations with different forces present some differences, it is quite clear that the experimental B(GT) distribution can only be reproduced assuming a prolate deformation as shown on the left-hand side of the figure. On

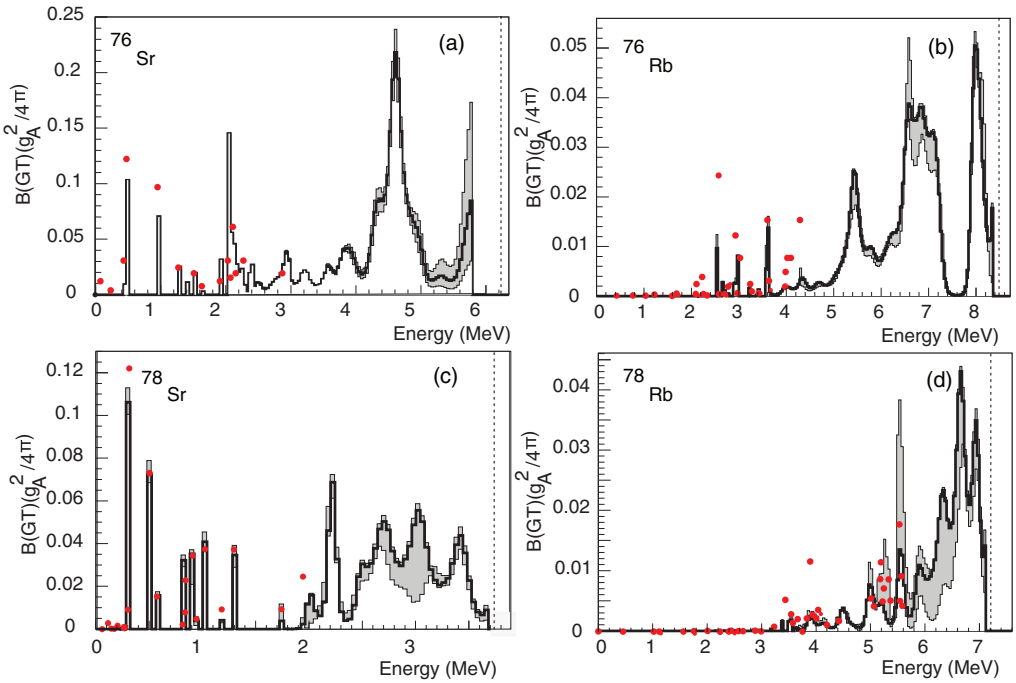

FIG. 7. (Color online) B(GT) distribution in the beta-decay of ^{76}Sr [6], ^{76}Rb, ^{78}Sr, and ^{78}Rb as a function of the excitation energy in the daughter nucleus (solid line) using the TAS method. The shaded areas indicate the range of errors. The B(GT) distributions, using the results of high resolution spectroscopy (red dots) are also shown. The dotted vertical lines indicate the positions of the Q_{EC} values.

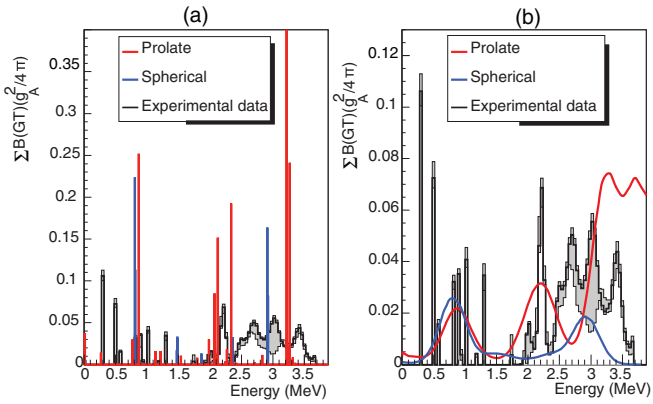

FIG. 9. (Color online) Experimental B(GT) distribution for ^{78}Sr resulting from this work compared with QRPA calculations for prolate and spherical shapes of ^{78}Sr using the SG2 Skyrme force [15]. It should be noted that in (b) the same theoretical distribution from (a) has been folded with a 0.5 MeV width Gaussian in order to simulate the fragmentation of the strength.

the right-hand side the experimental results are compared with similar calculations for the spherical case. From this comparison it becomes very clear that the parent state is prolate. This is in agreement with previous literature studies [38–40] and reinforces the discussion presented in [19]. It also provides another example, in addition to the ^{74}Kr and ^{76}Sr cases, that confirms that this kind of comparison can be used to deduce ground state deformations in the region.

If ^{76}Sr and ^{78}Sr are both prolate one might anticipate naively that, since the only change is a couple of extra neutrons, the B(GT) distributions will be similar. If we examine Fig. 11 where the accumulated B(GT) distributions for both even-even and odd-odd cases are shown, we see that this is indeed the case up to 3.7 MeV excitation in the daughter nucleus, the Q_{EC} value in ^{78}Sr. Above 3.7 MeV, there is strong feeding at 4–5 MeV in the decay of ^{76}Sr, whereas in ^{78}Sr this energy range is cut off by the Q_{EC} window as shown in Fig. 7 and we can say nothing about it.

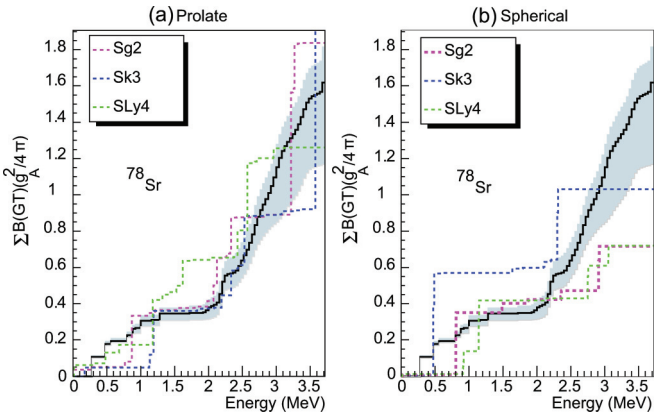

FIG. 10. (Color online) Accumulated experimental B(GT) distribution (solid line) compared with QRPA calculations for prolate (a) and spherical (b) shapes of ^{78}Sr using the SG2, Sk3, and SLy4 Skyrme forces [15].

B. Odd-odd nuclei

Unfortunately there are no similar theoretical calculations for the decay of the odd-odd nuclei. We will now try to draw some conclusions from the comparison of their B(GT) distributions with the corresponding even-even case. Figure 11 shows the accumulated B(GT) distributions for both the even-even and odd-odd cases.

We discuss the decay of the odd-odd $^{76-78}$Rb nuclei in qualitative terms by considering the possible types of transition, which are illustrated graphically in Fig. 12. Rather than the differences between the decay of ^{76}Rb and ^{78}Rb that certainly exist, we prefer to stress the similarities between the two decays, as well as the similarities with the even-even corresponding decays. In the upper right side of Fig. 12 we show the decay of the even-even case into the odd-odd daughter nucleus [diagram (a)]. This case involves the transformation of one proton in an occupied orbital into a neutron in an unoccupied orbital (note that in the present case, since we are talking about Nilsson orbitals which can be occupied by two particles at most, there is no difference between a "particle" and a "hole"). We will use this terminology since it is easier to explain what happens in β decay. The final state is a proton-neutron two-quasiparticle (2qp) state in the odd-odd nucleus. The excitation energy of the state populated is essentially the single-particle orbit energy difference of the two valence particles with respect to the ground state (plus the residual nucleon-nucleon residual interaction which we will neglect in the present discussion for simplicity).

In the odd-odd decay there are three different possibilities which are expected to lie in three different excitation energy regions:

Diagram (b) of Fig. 12 considers the transformation of the unpaired proton in the parent nucleus into a neutron in the daughter which occupies the same orbital as that of the odd neutron in the parent. In this case the final state results in two paired protons and two paired neutrons coupled to zero (0qp state) in the even-even daughter nucleus. This final state would correspond to the 0^+ ground state in the daughter nucleus. In the ^{76}Rb parent case, the ground state has a $(\pi[301]3/2^- - \nu[422]5/2^+)1^-$ configuration [41] and therefore this decay is not allowed. On the other hand, the ^{78}Rb parent is assumed to have a $(\pi[312]3/2^-$-$\nu[301]3/2^-)0^+$ configuration, as concluded in [19]. This decay would be isospin forbidden and would only occur if isospin mixing in the parent ground state was considered. As discussed above the analysis of the TAS data for ^{78}Rb confirm no strength in the gs-to-gs beta decay. Therefore the decay considered in diagram (b) is not possible for either of the two cases studied here, but for different reasons.

Diagram (c) shows two possible decays: either the transformation of the odd proton from the parent ground state into a neutron in a different orbital from the ground state or the proton from a different orbital from the ground state into a neutron in the same orbital occupied by the odd neutron in the parent state. This results in a final state of two-particle character [two unpaired valence protons or neutrons (2qp states) not coupled to zero in the daughter nucleus]. Relative to the daughter ground state, these states require enough energy to break the proton or the neutron pair plus the excitation energy of the

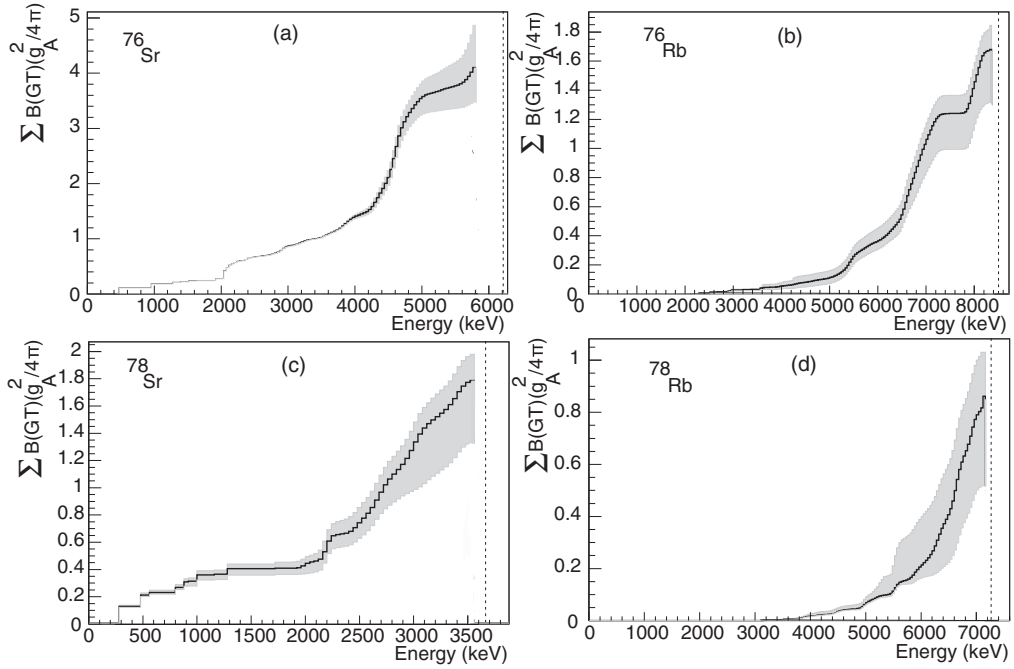

FIG. 11. Accumulated B(GT) for ^{76}Sr [6], ^{76}Rb, ^{78}Sr and ^{78}Rb as a function of the excitation energy in the daughter nucleus using the TAS method. The vertical dotted lines indicate the position of the Q_{EC} value. It should be noted that the analysis can be carried out up to values close to the Q_{EC}, namely up to the point where the number of counts is too small to provide useful information.

nucleons involved. Since a typical pairing gap for protons and neutrons in these nuclei is between 1 and 1.5 MeV, these excitations are possible beyond 2 or 3 MeV.

Diagram (d) shows the case in which the valence proton and neutron in the parent ground state act as spectators in the decay. One proton different from the unpaired one in the parent ground state gets transformed into a neutron occupying an orbital different from that of the unpaired one in the parent. Relative to the even-even ground state this is a four-particle (4qp) excitation with two unpaired protons and two unpaired neutrons, and requires the energy to break two pairs plus the corresponding single-particle energies. From the point of view of the transformation of the parent ground state, the beta decay is identical to diagram (a) except for the blocking imposed by the unpaired proton and neutron spectators. Consequently this strength should be similar to that of the even-even case but shifted by four times the energy gap if they have similar deformations.

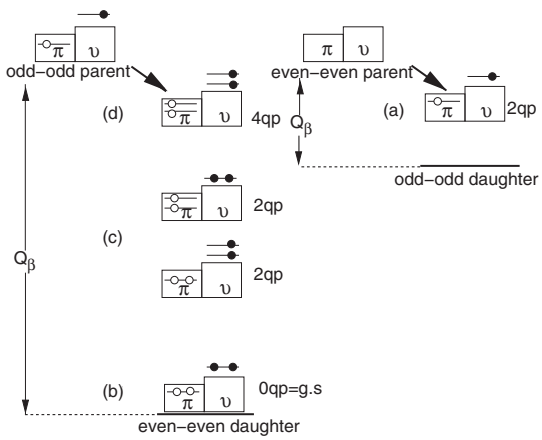

FIG. 12. Possible β decays in an odd-odd and even-even nucleus shown in an schematic way.

We can see that the decays of the odd-odd nuclei ^{76,78}Rb shown in Fig. 11 are quite similar. In both cases, there is practically no strength below 4 MeV. The strength slightly increases in the range 5–6 MeV and then increases rapidly for higher excitation energies. The structure beyond 7 MeV cannot be compared because of the smaller energy window in the case of the longer lived ^{78}Rb, but at this energy the accumulated strength in the two cases is comparable.

Figure 13 shows the B(GT) strength of ^{76}Sr and ^{76}Rb in the upper panel (I) and ^{78}Sr and ^{78}Rb in the lower panel (II), with the B(GT) of both Sr isotopes shifted 4.5 MeV with respect to the Rb isotopes. This shift in energy is approximately the same as the energy required to break two pairs. As explained above, the decay shown in diagram (b) in Fig. 12 is not possible for either ^{76}Rb or ^{78}Rb. In both cases most of the strength lies at high energies, which corresponds to the process drawn schematically in diagram (d). This is what one would expect since the number of possible orbitals participating in (d) is larger than in case (c). In addition, it can be observed that the strength due to the process described by diagram (c) in Fig. 12 seems larger in the decay of ^{76}Rb than in ^{78}Rb. This must be due to differences in the orbital configurations for the two cases. Since there are no microscopic calculations, no more conclusions have been drawn.

Using the lower panel (II) of Fig. 13, one can compare the decays of ^{78}Sr and ^{78}Rb and check whether the strength observed in ^{78}Sr, corresponding to diagram (a), is similar to the strength observed in ^{78}Rb decay at high energy in diagram (d).

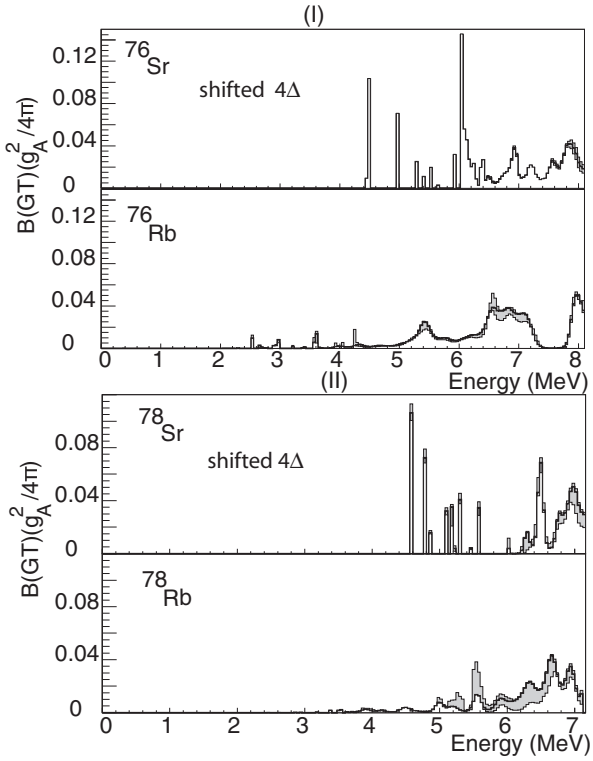

FIG. 13. The upper graph (I) shows a comparison between the B(GT) distributions of ^{76}Rb and ^{76}Sr. The latter has been shifted by ∼4.5 MeV which is approximately the energy required to break two pairs (Note: Δ here represents the pairing energy). The lower graph (II) shows the same for the ^{78}Sr and ^{78}Rb cases.

It can be seen that indeed the shape of the strength is similar in the range 5.5 to 7 MeV. However the strength lying within that region is smaller, which can be explained by the blocking effect of the spectator orbitals in the case of the odd-odd decay. What can be concluded from this comparison is that in general terms the structures of the ^{78}Sr and ^{78}Rb ground states are similar, which points to a prolate deformation. The same kind of comparison is not so conclusive in the ^{76}Rb case though, as seen in the upper graph (I) of Fig. 13. One possible reason might be that in the $N = Z$ ^{76}Sr one expects a maximum in the deformation due to the reinforcement of the 38 prolate gap for protons as well as neutrons. However, we can clearly conclude that most of the strength observed in the decay of ^{76}Rb is due to the decay represented by diagram (d), in agreement with our simplified scheme.

V. CONCLUSIONS

A study of the β decays of ^{78}Sr and ^{76,78}Rb using the Lucrecia spectrometer at ISOLDE has been carried out. From the analysis of the data, the intensities and B(GT) distributions have been deduced. The comparison of the B(GT) distribution of ^{78}Sr with HF+BCS+QRPA calculations has confirmed the prolate shape of its ground state. This is in agreement with our previous paper on ^{78}Sr beta decay. General conclusions have been drawn for the cases of the odd-odd nuclei, ^{76}Rb and ^{78}Rb, based on a comparison with the corresponding even-even nuclei. No theoretical calculations exist at the moment for the odd-odd cases. In this article we give the measured values for the B(GT) in the odd-odd decays so that a comparison with theory can be made in the future. We believe that the effort put into this series of experiments has contributed to a better mapping of ground state deformation for $N \sim Z$ nuclei in the $A \approx 80$ region.

ACKNOWLEDGMENTS

This work was supported in part by the Spanish MEC under Grant No. FPA2005-03993 and Formacion Profesorado Universitario Grant No. FPA2003-4041. It was also supported by MICINN Grants No. FPA2008-06419-C02-01, No. FPA2009-07387, No. FPA2010-17142, No. FPA2011-24533, and No. FIS2011-23565, by CPAN CSD-2007-00042, Ingenio2010, and by the UK Science and Technology Facilities Council (STFC) Grant No. ST/F012012/1. The experiments were partly supported through EURONS No. 506065.

[1] P. J. Nolan and P. J. Twin, Annu. Rev. Nucl. Part. Sci. **38**, 533 (1988).
[2] J. Blons, Nucl. Phys. A **502**, 121 (1989).
[3] L. P. Gaffney *et al.*, Nature (London) **497**, 199 (2013).
[4] B. Rubio *et al.*, J. Phys. G: Nucl. Part. Phys. **31**, S1477 (2005), and references therein.
[5] S. G. Nilsson, Dan. Mat. Fys. Medd. **29**, 16 (1955).
[6] E. Nácher *et al.*, Phys. Rev. Lett. **92**, 232501 (2004).
[7] I. Hamamoto and X. Z. Zhang, Z. Phys. A **353**, 145 (1995).
[8] P. Sarriguren, E. Moya de Guerra, A. Escuderos, and A. C. Carrizo, Nucl. Phys. A **635**, 55 (1998).
[9] J. C. Hardy *et al.*, Phys. Lett. B **71**, 307 (1977).
[10] J. L. Tain and D. Cano-Ott, Nucl. Instrum. Methods A **571**, 719 (2007).
[11] J. L. Tain and D. Cano-Ott, Nucl. Instrum. Methods A **571**, 728 (2007).
[12] E. Poirier *et al.*, Phys. Rev. C **69**, 034307 (2004).
[13] A. Algora *et al.*, Phys. Rev. Lett. **105**, 202501 (2010).
[14] M. Fallot *et al.*, Phys. Rev. Lett. **109**, 202504 (2012).
[15] P. Sarriguren, Phys. Rev. C **79**, 044315 (2009).
[16] Ph. Dessagne *et al.*, Eur. Phys. J. A **20**, 405 (2004).
[17] A. Giannatiempo *et al.*, Phys. Rev. C **72**, 044308 (2005).
[18] G. K. Bavaria, J. E. Crawford, S. Calmawy, and J. E. Kitching, Z. Phys. A **302**, 329 (1981).
[19] A. B. Pérez-Cerdán *et al.*, Phys. Rev. C **84**, 054311 (2011).
[20] G. Audi, O. Bersillon, J. Blachot, and A. H. Wapstra, Nucl. Phys. A **624**, 1 (1997).
[21] M. Wang *et al.*, Chin. Phys. C **36**, 1603 (2012).
[22] H. L. Ravn *et al.*, Nucl. Instrum. Methods **123**, 131 (1975).
[23] R. Eder *et al.*, Nucl. Instrum. Methods B **62**, 535 (1992).
[24] J. C. Hardy and I. S. Towner, Phys. Rev. C **79**, 055502 (2009).
[25] J. C. Hardy and I. S. Towner, Nucl. Phys. News **16**, 11 (2006).
[26] N. B. Gove and M. J. Martin, Nucl. Data Tables A **10**, 205 (1971).

[27] D. Cano-Ott *et al.*, Nucl. Instrum. Methods A **430**, 333 (1999).
[28] http://geant4.cern.ch/.
[29] http://www-nds.iaea.org/RIPL-2.
[30] W. Dilg *et al.*, Nucl. Phys. A **217**, 269 (1973), and references therein.
[31] G. A. Bartholomew *et al.*, Adv. Nucl. Phys. **7**, 229 (1973).
[32] J. C. Hardy *et al.*, Phys. Lett. B **109**, 242 (1982).
[33] J. Kopecky and M. Uhl, Phys. Rev. C **41**, 1941 (1990).
[34] W. V. Prestwich *et al.*, Z. Phys. A **315**, 103 (1984).
[35] D. Cano-Ott *et al.*, Nucl. Instrum. Methods A **430**, 488 (1999).
[36] R. A. Kaye *et al.*, Phys. Rev C **54**, 1038 (1996).
[37] E. Nácher, Ph.D. thesis, Universitat de Valencia, 2004 (unpublished); E. Nácher *et al.* (unpublished).
[38] C. J. Lister, B. J. Varley, H. G. Price, and J. W. Olness, Phys. Rev. Lett. **49**, 308 (1982).
[39] F. Buchinger *et al.*, Phys. Rev C **41**, 2883 (1990).
[40] P. Möller, J. R. Nix, W. D. Myers, and W. J. Swiatecki, At. Data Nucl. Data Tables **59**, 185 (1995).
[41] A. Harder *et al.*, Phys. Rev. C **51**, 2932 (1995).